Wide-field Surface-Enhanced Coherent Anti-Stokes Raman Scattering Microscopy

Cheng Zong‡, Ran Cheng‡, Fukai Chen, Peng Lin, Meng Zhang, Zhicong Chen, Chen Yang*, Ji-Xin Cheng*

Supporting Information Placeholder

ABSTRACT: Surface-enhanced Raman scattering (SERS) spectroscopy has been used extensively to study biology, chemistry, and materials. However, a point-by-point SERS mapping is time-consuming, taking minutes to hours for large-scale imaging. Here, we report a wide-field surface-enhanced coherent anti-Stokes Raman scattering (WISE-CARS) microscopy for monitoring nanotags in live cells and label-free detection of metabolic molecules. The WISE-CARS microscope achieves an imaging speed as fast as 120 frames per second for a large field of view of 130 μm × 130 μm. By spectral focusing of femtosecond lasers, a hyperspectral WISE-CARS stack of 120 frames can be acquired with a spectral resolution of 10 cm^{-1}, where over 1 million Raman spectra are parallelly recorded within 0.5 seconds. As applications, we demonstrate time-lapse, 3D WISE-CARS imaging of nanotags in live cells as well as label-free detection of adenine released from *S. aureus*.

1. INTRODUCTION

Surface-enhanced Raman spectroscopy (SERS) is a powerful vibrational spectroscopy technique that allows for highly sensitive structural detection of low concentration analytes even down to single molecule level.[1-2] Due to the localized surface plasmon resonance (LSPR), an extremely large local electromagnetic field is generated on the metal surface to amplify the Raman signals of molecules which closely associated with the nanostructure.[3-4] However, most of the instrumentations used for SERS imaging are equipped with a CCD detector which typically operates with acquisition rate on the order of 1 Hz and rely on the mechanical scanning process.[5] For large-area imaging, the time-consuming point-by-point scanning process with an acquisition time of few seconds often takes minutes to hours for mapping the SERS spectra of a sample.[6]

With high-speed cameras and tunable filters, wide-field SERS imaging has been developed to meet the need for large-scale Raman imaging.[7-10] Among these technologies, wide-field hyperspectral imaging is achieved by utilizing tunable band-pass filters, such as liquid crystal tunable filters [9-10] or angle-dependent filters[7-8], to scan a Raman spectral window. Yet, the spectral resolution of tunable filters is limited at tens of wavenumbers. In addition, the wavelength tuning speed per wavelength step is about hundreds of milliseconds which limits the hyperspectral imaging speed.

Coherent anti-Stokes Raman scattering (CARS) has already demonstrated great potentials for biomedical imaging.[11-15] Compared with spontaneous Raman microscopy, CARS microscope is typically carried out by point-scanning the sample with a point detector (photomultiplier tubes and avalanche photodiode) which can achieve much faster acquisition rate (1 MHz). Thus, CARS microscopy enables high-speed chemical imaging of living systems at video rate.[16] To achieve higher sensitivities, surface plasmon resonance effect has been employed to enhance CARS signals[17-20] and the single molecule detection has been verified via surface-enhanced CARS (SECARS).[21-23] While most of SECARS imaging were achieved in scanning mode, where the imaging speed is limited, especially for the hyperspectral data acquisition.

To achieve a faster imaging speed, alternative excitation geometries based on wide-field illumination have been developed. Early wide-field CARS setup used a dark-field condenser to focus pump light and counterpropagating Stokes beam to satisfy phase-matching condition.[24] Later, simper illumination geometries were adapted such as defocused laser beams[25] and high-incidence illumination schemes[26-28]. Such non-phase matched illuminations rely on the strongly scattering samples to redirect the light path. The video-rate wide-field CARS imaging and even single-shot imaging of biological samples have been demonstrated.[25, 28] However, all their schemes are based on single-color CARS.[29] High-speed hyperspectral CARS imaging with wide-field illumination was not fully demonstrated. Recently, to further increase the detection sensitivity, Potma *et. al.* employed wide-field evanescent illumination in CARS microscopy, where surface plasmon polariton (SPP) from 30 nm gold film enhanced the CARS signal of organic films and dried cells.[30-31] However, the coherent SPP induces flares and interfering pattern in the image and cannot be used for imaging into a live cell.

Here, we demonstrate a wide-field surface-enhanced coherent anti-Stokes Raman scattering (WISE-CARS) microscope that enables ultra-high-speed imaging of living cells. Our method takes full advantages of SECARS. First, the power density in SECARS is 1000 times lower than that in conventional CARS microscopy without plasmonic enhancement.[32] This low power requirement opens the opportunity for wide-field illumination and parallel data collection. Second, the main issue in wide-field CARS microscopy, the phase-matching condition over the whole field of view,[24] is relaxed in WISE-CARS. Because SECARS is excited by the local electric fields from nanostructures, the signal can be generated without controlling the direction of the excitation beams to match the far-field phase matching condition. Third, we utilize a spectral focus approach for fast tuning the beating frequency between pump and Stokes beams, which allows ultra-high-speed hyperspectral CARS imaging. As applications, we demonstrate hyperspectral SECARS imaging of an aggregated Au NPs substrate with 120 frames per second (fps). Then, we illustrate the system's capability by WISE-CARS imaging of live cells at 60 fps and 3D imaging of nanotags in live cells within 1 second. Furthermore, we demonstrate a label-free detection of adenine, an endogenous biomolecule released from *S. aureus* bacteria, via WISE-CARS microscopy.

2. EXPERIMENTAL SECTION

2.1. Hyperspectral wide-field CARS microscope. The schematic of the hyperspectral wide-field CARS microscope is shown in **Figure 1a**. In brief, a femtosecond laser (Spectra-physics, InSight DS) with 80 MHz repetition rate provides a tunable pump (680-1350 nm) beam and a fixed Stokes (1040 nm) beam. The pump and Stokes beams are combined on a dichroic beam splitter and then both are chirped by 5 × 15 cm SF glass rods for spectral focusing purpose. For equally stretching, the Stokes pulse is chirped by an additional 15 cm SF glass rod before combination. Using such chirping condition, the spectral resolution of our setup is 10 cm^{-1}.[33] Then combined beams are expand 2 times by a lens pair for increasing the field of view. The combined beams are focused with a 250 mm achromatic lens on the back focal plane of a 20 × 0.4 NA objective (Olympus) to provid wide field illumination. The illuminate area at the sample is around 130 μm × 130 μm (**Figure 1b**). After the sample, the forward scattered beam is collected by a 60 × 1.2 NA water immersion objective (Olympus). The sample image is projected onto the CMOS camera (Grasshopper3, FLIR) through a tube lens with a focal length of 180 mm. The CMOS camera allows imaging speeds as high as 120 fps at a resolution of 1224×1024 pixels, with a pixel size of 0.13 μm. Bandpass filters before the camera blocks the excitation light, while the CARS signal passes through. A LED light is used for a bright view imaging.

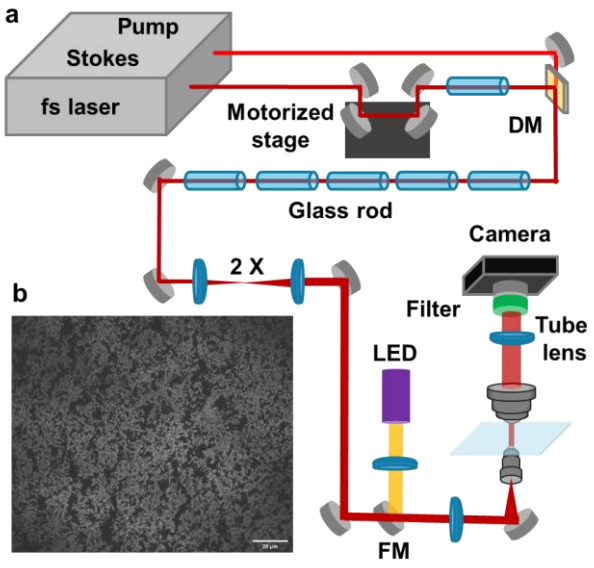

Figure 1. The hyperspectral wide-field SECARS microscope. a) Schematic. DM: dichroic mirror; FM: flipper mirror. b) The brightfield view of the aggregated Au NPs substrate illuminated by the pump laser.

To obtain hyperspectral information, a motorized linear stage is installed in the Stokes beam for tuning the delay between chirped pump and Stokes beams. The motorized stage and the CMOS camera are synchronously triggered. When the camera is exposed, the motorized stage starts a uniform linear motion at a specific speed. For example, with a commonly used delay distance =1.2 mm, the velocity of stage is 1.2 mm per second and the framerate of camera is 60 fps. In this condition, the hyperspectral CARS data cube with 60 Raman channels can be obtained in 1 second.

To obtain 3D sections, a piezoelectric objective lens positioner (MIPOS100 piezosystem jena) is used to control the focus of the collection objective. The piezo positioner and camera also synchronized. The piezo positioner scans from bottom to top at a uniform speed when the camera captures images.

2.2. Preparations of Au NPs for WISE-CARS detection. The Au NPs colloid is prepared by the citrate reduction method, resulting in particles with a diameter of 40 to 50 nm. Three different samples are prepared for WISE-CARS imaging. The first sample is an aggregated Au NPs substrate for larger area imaging. The 0.5 mL of Au NPs colloidal suspension is concentrated to 2–4 μL by centrifuging, which is then added to the 5 μL analyte solution. The analyte solution induces the aggregation of Au NPs. The aggregated Au NPs are dropped on a cover glass, followed by vacuum drying to obtain the substrate for SECARS imaging. Second, 4-mercaptopyridine (Mpy)-modified Au nanotags for live cells imaging. The as-prepared 5 mL Au NPs are subsequently functionalized with Mpy by adding 50 μL of 54 μM Mpy aqueous solution under vigorous shaking. To increase the stability of Mpy-functionalized Au NPs colloid, 50 μL of 2 % bovine serum albumin aqueous solution is added dropwise under vigorous stirring and is kept shaking for 15 min.[34] Third, as described in our previous paper,[32] an self-assembled Au NPs substrate is prepared for bacterial measurement. In brief, homogeneous Au NPs with a diameter of 60 nm are synthesized by two-step seed-mediated growing method. The cleaned cover glass is silanized in 10% (v/v) of (3-aminopropyl)- trimethoxysilane ethanol solution for 24 hrs and then baked at 110 °C for 2 hrs. Finally, the cover glass is immersed in the above 60 nm Au NPs solution for 20 hrs to assembled Au NPs.[35]

2.3 Cell culture and sample preparation for live cell imaging. T24 cells are cultured in DMEM medium with 10 % fetal bovine serum and 1 % penicillin-streptomycin. The suspended T24 cells are seeded on a glass bottom dish and cultured 48 hours for the attachment. 1 mL of nanotags are centrifuged and the supernatant is removed. The concentrated nanotags are added into the culture medium to interact with cells for 8 hours. After that, the culture medium is discarded, and the cells are washed three times by phosphate-buffered saline (PBS) to remove the free nanoparticles. Finally, 2 mL of PBS is added into the culture dish again before WISE-CARS imaging.

S. aureus cells are cultured in Mueller Hinton broth and are harvested at the log phase. The bacteria are washed 3 times with 1 mL water. The bacterial pellet is suspended in 20 μL of water and 5 μL of the resulting bacterial suspension is dropped and dried onto the self-assembled Au NPs substrate. Samples are dried onto the Au substrate either immediately (0 h) or after 1 hr in order to demonstrate the effect of the starvation stress response.

2.4. Data processing. The camera, motorized stage, and piezoelectric positioner are controlled by Matlab (MathWorks). The data are collected and processed by Matlab. BM4D is used to denoise the SECARS data.[36]

3. RESULTS

3.1. Hyperspectral WISE-CARS imaging of gold nanosubstrate. To demonstrate the hyperspectral WISE-CARS, we first show the results obtained from the Mpy-modified aggregated Au NPs substrate. The pump laser centered at 891 nm was employed to induce a SECARS spectra covering a window ranging from 1520 cm^{-1} to 1680 cm^{-1}. The pump and Stokes laser power both were both set to 150 mW. A hyperspectral data cube (1224×1024×120) was recorded with 60 fps. **Figure 2a** shows an SECARS image of Mpy-modified aggregated Au NPs substrate at 1577 cm^{-1}. The

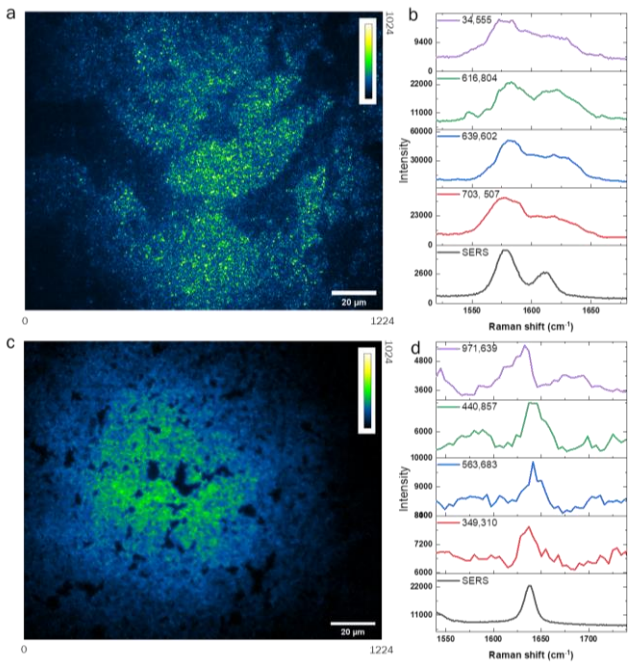

Figure 2. Hyperspectral WISE-CARS imaging of Au NPs substrate. a) The SECARS image of Mpy adsorbed on aggregated Au NPs substrate. b) The single-pixel SECARS spectra of Mpy and the SERS spectrum of Mpy (bottom). c) The SECARS image of ATTO740 adsorbed on aggregated Au NPs substrate. d) The single-pixel SECARS spectra of ATTO740 and the SERS spectrum of ATTO740 (bottom). The scale bar is 20 μm. The inside labels show the X–Y pixel coordinate where the spectra were recorded

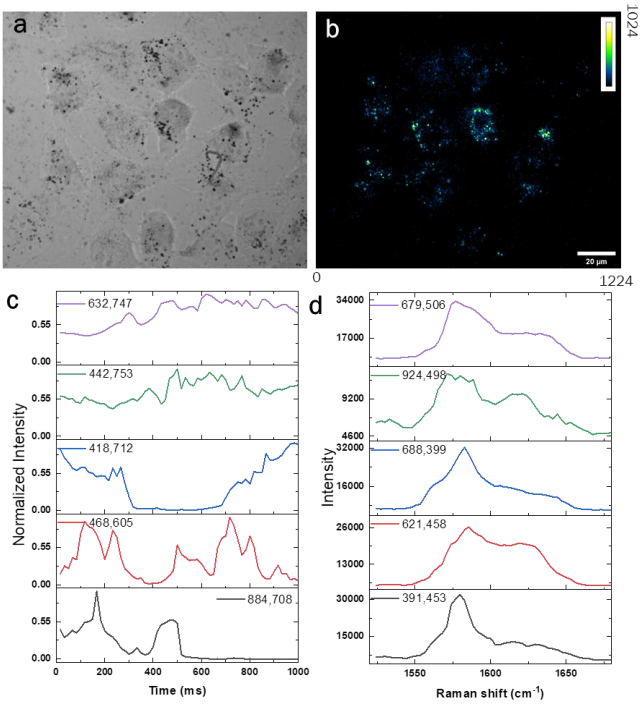

Figure 3. Hyperspectral WISE-CARS imaging of live cells. a) The bright view of T24 cells illuminated by LED. b) Corresponding SECARS imaging of T24 cells at 1577 cm^{-1}. c) The time-lapse of single cluster. d) the single-pixel SECARS spectra of nanotags in live cells. The scale bar is 20 μm The inside labels show the X–Y pixel coordinate where the spectra were recorded.

hyperspectral data cube was shown as in **Video 1**. The signal originated from total image area. The pattern shows the heterogeneity of Au NPs substrate. **Figure 2b** shows representative single pixel SECARS spectra of Mpy and SERS spectrum of Mpy (bottom). The two peaks at 1577 cm^{-1} and 1612 cm^{-1} can be observed in single pixel SECARS spectra. The relative intensity of these two peaks relates with the adsorbed conditions of Mpy on Au NPs.[35]

To further demonstrate the capability of high-speed hyperspectral imaging, we prepared the ATTO740 modified aggregated Au NPs substrate. To cover the desired spectral window, the pump beam was tuned to 888 nm. The power of pump and Stokes lasers both were 120 mW. With 120 fps imaging speed, we only took 0.5 s to obtain the hyperspectral data cube (1224×1024×60) of ATTO740 on Au NPs. In this condition, the the velocity of motorized stage was 2.4 mm per second. The SECARS imaging at 1637 cm^{-1} are shown in **Figure 2c**. **Figure 2d** presents the representative single pixel SECARS spectra and the SERS spectrum (bottom) of ATTO740 on Au NPs. The single peak at 1637 cm^{-1} is clearly observed in SECARS spectra and the SERS spectrum. Hence, we successfully demonstrate the capability of WISE-CARS to parallelly record over 1 million SECARS spectra in 0.5 s.

3.2. Dynamic WISE-CARS imaging of live cells. To demonstrate the capability of dynamic live cells imaging, we incubated Mpy-modified Au nanotags with T24 cells for 8 hours (**Figure 3a**). After 8 hrs incubation, the Au NPs were expected to be uptaked by endocytosis process and thereafter enclosed within endosomes or lysosomes.[37] To record the movements of nanotags, we choose the Raman signature band of Mpy molecules at 1577 cm^{-1}as a demonstration. The frame rate was 16.6 ms per a 1224 × 1024-pixel image. With frame acquisition time as short as 16.6 ms, a 60-frame video was recorded to show the movements of nanotags inside a live cell during 1 s period (see **Video 2**). **Figure 3b** shows an SECARS image of live T24 cells at 1577 cm^{-1}. The bright spots indicate the location of Au nanotags. As shown **Figure 3c**, the time-lapse observation provides spatiotemporal dynamic of nanotags such as spatial movements and intensity blinking, suggesting that rapid changes of nanoparticles in live cells at millisecond level. In addition, the SECARS signals of a part nanotags show significant intensity fluctuations while others show a relative stable change. This result suggests that the nanoparticles may exist different conditions inside live cells.

To record the hyperspectral SECARS imaging in live cells, we simultaneously scanned the delay stage and recorded imaging in 1 second. The frame rate was 60 fps. The hyperspectral SECARS spectra in live cells shows in **Video 3**. **Figure 3d** presents the representative single pixel SECARS spectra. The two peaks of Mpy which located 1577 cm^{-1} and 1612 cm^{-1} are clearly observed in single pixel spectra. The ratio between two peaks is different because the Mpy is a pH-sensitivity molecule. The different ratios indicate that the nanotags exist in different stage of endocytic process like early endosome (pH 6.0–6.5), late endosomes (pH 5.5) and lysosome (pH 4.0- 5.0).[37] This result indicates that the hyperspectral WISE-CARS could high-speed monitor chemical sensors in live cells.

3.3. 3D WISE-CARS imaging of live cells. To demonstrate the 3D imaging ability of WISE-CARS imaging, the live T24 cells were treated with Mpy-modified Au NPs nanotags for 8 hrs. A

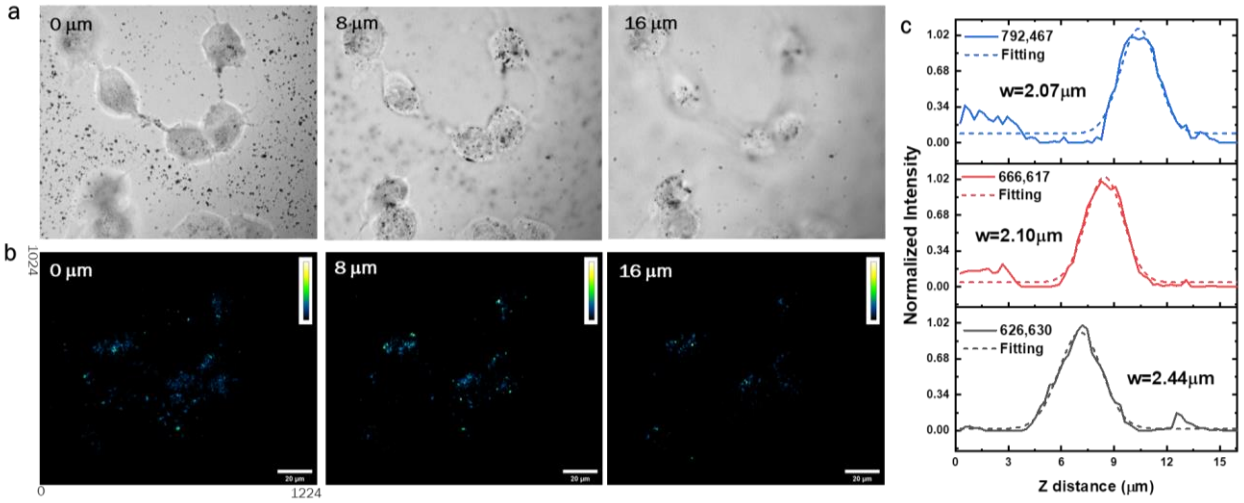

Figure 4. 3D WISE-CARS imaging of live cells. a) The bright views of T24 cells at different focus plane. b) Corresponding SECARS imaging of T24 cells at 1577 cm^{-1}. c) The z-profiles of single clusters in T24 cells. The scale bar is 20 μm. The inside labels show the X–Y pixel coordinate where the spectra were recorded.

piezoelectric objective scanner was used to control the focal plane. At first, the objective was focus on the bottom (0 μm) of the glass bottom dish. The focus plane continuously moved up to 16 μm in 1 second. At the same time, the camera recorded bright images (**video 4**) or the SECARS images (**video 5**) with 60 fps. Total 60 3D sections were recorded, and each z-step was 267 nm. **Figure 4a & b** show the bright view and corresponding WISE-CARS images at 3 z-positions at bottom (0 μm), middle (8 μm) and top (16 μm). At bottom, the SECARS image shows the nanotags inside cells and the nanotags attached on the glass. When the focal plan moves up, the SECARS signals from nanotags outside cells fade away. When the focus plane at the center of cell, most of signals origin from the nanotags in the cells. The 3D images of WISE-CARS show the distribution of nanotags in different layers. The 3D projection (**video 6**) shows the 3D distributions of nanotags in live cells. Our WISE-CARS only takes 1 second to obtain the live cells 3D imaging. To estimate the depth resolution of our setup, we select 3 small particles in the cells and plot their z-profiles as shown in **Figure 4c**. The width of z-profiles of nanotags are c.a. 2 μm resulting from gaussian fitting. This result indicates that the depth resolution of our setup will not be worse than 2 μm which is better than that of wide-field CARS microscopy (>10 μm).[25] This result indicates that WISE-CARS has a great potential to real-time visualize 3D distribution of nanotags in cells.

3.4. Label-free biomolecule detection by WISE-CARS microscopy. To demonstrate the label-free endogenous biomolecule detection of the WISE-CARS microscopy, adenine is selected as a proof-of principle molecule. The pump beam was tuned to 967 nm to cover the desired vibrational region around 724 cm^{-1}. The pump and Stokes laser power were both 150 mW. First, hyperspectral data cubes from the adenine ($N^{14}A$) and adenine-1, 3-$^{15}N_2$ ($N^{15}A$) modified aggregated Au NPs samples were recorded with 60 fps. **Figure 5a** shows the SECARS image of $N^{14}A$ at 738 cm^{-1}. As shown in **Figure 5b**, SECARS spectra of $N^{14}A$ and $N^{15}A$ show clearly distinguishable Raman bands centered at 738 cm^{-1} and 727 cm^{-1}, respectively. This result indicates the spectra resolution of WISE-CARS is about 10 cm^{-1}. Then, the single pixel SECARS spectra of $N^{14}A$ are shown in **Figure 5c**.

In addition, we measured the stress response of *S. aureus* cells. *S. aureus* cells can secret adenine, a purine degradation product, when they exposure to a no-nutrient, water-only environment. The bacterial suspensions were dropped on the self-assembled Au NPs substrates and were dried in 10 min. The SECARS spectra were background-subtracted by the airPLS method.[38] The SECARS spectrum of *S. aureus* after 1 h starvation is showed in **Figure 5d** and the observed spectra closely resemble the SECARS spectrum of adenine in **Figure 5b**. In contrast, the SECARS spectra obtained without waiting time do not display adenine-like Raman peak. The

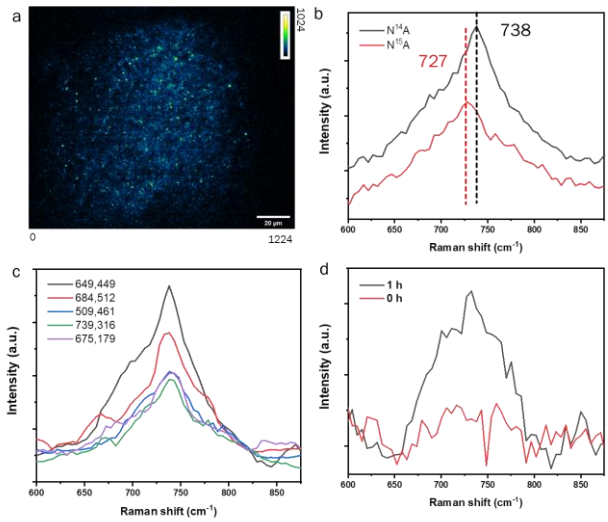

Figure 5. WISE-CARS detection of biomolecules. a) The SECARS image of adenine adsorbed on aggregated Au NPs substrate at 738 cm^{-1}. b) SECARS spectra of $N^{14}A$ and $N^{15}A$. c) The single pixel spectra of $N^{14}A$. The labels show the X–Y pixel coordinate where the spectra were recorded. d) The background corrected SECARS spectra of *S. aureus* with (1 h) and without (0 h) starvation.

results match well with the previous results.[39-40] This result indicates the WISE-CARS microscopy opens a great opportunity for label-free detection of biological molecules. Moreover, the WISE-CARS can sample millions of pixels on the sample in 1 second which avoids pixel-dependent fluctuations and collectively allows quantitative chemical analysis.

4. DISCUSSION

In this work, we developed the WISE-CARS method for real-time observing the dynamic spatiotemporal distribution of nanotags in live cells and label-free detection of endogenous biomolecules. Unlike the scanning-based microscopy, the acquisition time in the wide-field imaging system is virtually independent of the pixel number. Therefore, we successfully achieve 120 fps CARS imaging (5 times of video rate) with a large field of view (over 130 μm) and high spatial resolution (1224 × 1024 pixel). SERS based wide-field imaging needs a sophisticated tunable filter for the acquisition of hyperspectral data. The tunable filter will limit the tuning speed and spectral resolutions. While with the spectral focus approach, the spectral tuning of WISE-CARS could be very fast by simply changing the time delay between two laser pulses via a motorized stage. In this way, WISE-CARS can simultaneously obtain over 1 million spectra in 0.5 s with a 10 cm^{-1} spectral resolution, which is state of art of hyperspectral imaging speed.

In addition, combined with plasmon-enhanced effect, the WISE-CARS microscopy only requires ultra-lower power density for exciting a CARS process. The estimated average laser density in WISE-CARS is 0.015 mW / μm^2, which is 30 times lower compared to the previous laser-scanning SECARS and 4 orders lower than than in laser-scanning CARS. Such low illumination density opens a great opportunity to implement wide-field CARS imaging with standard high-repetition rate lasers and low pulse energies. High repetition rate laser can help to achieve a high-speed imaging. In addition, lower pulse energies also help to reduce the potential photodamage as may occur when illuminating with high energy pulses in conventional CARS microscopy.[28] Recent literature reported of wide-field SPP-mediated CARS to image lipid solid sample and dry cells. Although a gold film was used to uniformly amplify the signal generation, it also introduced imaging artifacts from the SPP propagations. In addition, SPP only enhanced detection of cell membrane region in close proximity (100 nm) of the gold film.[30] Here, we used the LSPR effect from nanoparticles that can amplify the Raman signal inside live cells and enable to generate 3D imaging. Moreover, the enhancement performance of LSPR allows the amplification with a factor of 10^{10},[32] which is 3 orders of magnitude stronger than SPP enhancement.[31]

Besides SECARS, an alternative method that combined coherent Raman microscopy and plasmon enhanced effect is Plasmon-enhanced stimulated Raman scattering (PESRS) microscopy for the ultra-sensitive imaging.[39, 41] However, implementing SRS is more complex in the wide-field geometry. First, in SRS measurement, the incident beam should be directly detected by the camera. The power saturation threshold of a camera normally is smaller than 10 mW. In this way, the power density on the sample is too low to effectively excite signals. Second, PESRS did not show a clear advantage over SECARS. PESRS displays dispersive line shapes and its enhancement factor is lower than SECARS.[32]

This proof-of principle study on WISE-CARS may serve as a starting point for further investigation using this plasmon-enhanced nonlinear vibrational imaging technique. Our method can be a promising technique toward ultrafast 3D imaging of spatiotemporal dynamics of small molecules in live cells with single molecule sensitivity.[21-22] In addition, when antibodies or other target-specific ligands are conjugated to plasmonic nanotags which are labeled with spectrally distinct Raman reporters,[20] high-speed super-multiplex imaging can be envisioned through our hyperspectral WISE-CARS microscopy.

ASSOCIATED CONTENT

Supporting Information

The Supporting Information is available free of charge on the ACS Publications website. The GIF video of hyperspectral SECARS from Mpy modified nanosubstrate. The GIF video of hyperspectral SECARS from live cells. The GIF video of real time monitoring of nanotags in cells. The GIF video of 3D section of nanotags in cells. The GIF video of 3D projection of nanotags in cells.

AUTHOR INFORMATION

Corresponding Authors

Ji-Xin Cheng — *Department of Electrical and Computer Engineering, Department of Biomedical Engineering, Department of Chemistry, Boston University, Boston, Massachusetts, 02215, USA; Email: jxcheng@bu.edu*

Chen Yang — *Department of Chemistry, Boston University, Boston, Massachusetts, 02215, USA; Email: cheyang@bu.edu*

Authors

Cheng Zong‡ — *Department of Electrical and Computer Engineering, Boston University, Boston, Massachusetts, 02215, USA*

Ran Cheng‡ — *Department of Chemistry, Boston University, Boston, Massachusetts, 02215, USA*

Fukai Chen — *Department of Biomedical Engineering, Boston University, Boston, Massachusetts, 02215, USA*

Peng Lin — *Department of Electrical and Computer Engineering, Boston University, Boston, Massachusetts, 02215, USA*

Meng Zhang— *Department of Electrical and Computer Engineering, Boston University, Boston, Massachusetts, 02215, USA*

Zhicong Chen — *Department of Electrical and Computer Engineering, Boston University, Boston, Massachusetts, 02215, USA*

‡These authors contributed equally.

Author Contributions

Experiments were designed by C.Z. and J.X.C.. C. Z. developed the WISE-CARS microscopy with the help of P.L.. The WISE-CARS experiments were conducted by C.Z. and R.C.. R.C. and C.Z. synthesis nanoparticles and nanosubstrates. Data analysis was executed by C.Z.. F.C. and Z.C prepared live cells samples. M.Z. prepared bacteria samples. C.Z. and R.C. wrote the paper, revised by J.X.C. and C.Y.. All authors commented on the paper.

Notes

The authors declare no competing financial interests.

ACKNOWLEDGMENT

This work was supported by NIH R35 GM136223 NSF CHE1807106 to J.X.C.

REFERENCES

[1] Zong, C.; Xu, M.; Xu, L.-J.; Wei, T.; Ma, X.; Zheng, X.-S.; Hu, R.; Ren, B., Surface-Enhanced Raman Spectroscopy for Bioanalysis: Reliability and Challenges. [J] *Chemical Reviews* **2018,** *118*, 4946-4980.

[2] Langer, J.; Jimenez de Aberasturi, D.; Aizpurua, J.; Alvarez-Puebla, R. A.; Auguié, B.; Baumberg, J. J.; Bazan, G. C.; Bell, S. E. J.; Boisen, A.; Brolo, A. G.; Choo, J.; Cialla-May, D.; Deckert, V.; Fabris, L.; Faulds, K.; García de Abajo, F. J.; Goodacre, R.; Graham, D.; Haes, A. J.; Haynes, C. L.; Huck, C.; Itoh, T.; Käll, M.; Kneipp, J.; Kotov, N. A.; Kuang, H.; Le Ru, E. C.; Lee, H. K.; Li, J.-F.; Ling, X. Y.; Maier, S. A.; Mayerhöfer, T.; Moskovits, M.; Murakoshi, K.; Nam, J.-M.; Nie, S.; Ozaki, Y.; Pastoriza-Santos, I.; Perez-Juste, J.; Popp, J.; Pucci, A.; Reich, S.; Ren, B.; Schatz, G. C.; Shegai, T.; Schlücker, S.; Tay, L.-L.; Thomas, K. G.; Tian, Z.-Q.; Van Duyne, R. P.; Vo-Dinh, T.; Wang, Y.; Willets, K. A.; Xu, C.; Xu, H.; Xu, Y.; Yamamoto, Y. S.; Zhao, B.; Liz-Marzán, L. M., Present and Future of Surface-Enhanced Raman Scattering. [J] *ACS Nano* **2020,** *14*, 28-117.

[3] Willets, K. A.; Van Duyne, R. P., Localized surface plasmon resonance spectroscopy and sensing. [J] *Annu. Rev. Phys. Chem.* **2007,** *58*, 267-297.

[4] Ding, S.-Y.; Yi, J.; Li, J.-F.; Ren, B.; Wu, D.-Y.; Panneerselvam, R.; Tian, Z.-Q., Nanostructure-based plasmon-enhanced Raman spectroscopy for surface analysis of materials. [J] *Nature Reviews Materials* **2016,** *1*, 1-16.

[5] Lindquist, N. C.; Brolo, A. G., Ultra-High-Speed Dynamics in Surface-Enhanced Raman Scattering. [J] *The Journal of Physical Chemistry C* **2021,** *125*, 7523-7532.

[6] Chen, Y.; Ren, J.-Q.; Zhang, X.-G.; Wu, D.-Y.; Shen, A.-G.; Hu, J.-M., Alkyne-Modulated Surface-Enhanced Raman Scattering-Palette for Optical Interference-Free and Multiplex Cellular Imaging. [J] *Analytical Chemistry* **2016,** *88*, 6115-6119.

[7] Wang, M.; Zhang, C.; Yan, S.; Chen, T.; Fang, H.; Yuan, X., Wide-Field Super-Resolved Raman Imaging of Carbon Materials. [J] *ACS Photonics* **2021**.

[8] Havener, R. W.; Ju, S.-Y.; Brown, L.; Wang, Z.; Wojcik, M.; Ruiz-Vargas, C. S.; Park, J., High-Throughput Graphene Imaging on Arbitrary Substrates with Widefield Raman Spectroscopy. [J] *ACS Nano* **2012,** *6*, 373-380.

[9] Wang, L.; Dai, Y.; He, H.; Lv, R.; Zong, C.; Ren, B., Dynamic Raman imaging system with high spatial and temporal resolution. [J] *Review of Scientific Instruments* **2017,** *88*, 095110.

[10] Kim, J.; Nam, S. H.; Lim, D.-K.; Suh, Y. D., SERS-based particle tracking and molecular imaging in live cells: toward the monitoring of intracellular dynamics. [J] *Nanoscale* **2019,** *11*, 21724-21727.

[11] Cheng, J.-X.; Xie, X. S., Vibrational spectroscopic imaging of living systems: An emerging platform for biology and medicine. [J] *Science* **2015,** *350*.

[12] Liao, C.-S.; Cheng, J.-X., In situ and in vivo molecular analysis by coherent Raman scattering microscopy. [J] *Annual Review of Analytical Chemistry* **2016,** *9*, 69-93.

[13] Zhang, C.; Zhang, D.; Cheng, J.-X., Coherent Raman scattering microscopy in biology and medicine. [J] *Annual review of biomedical engineering* **2015,** *17*, 415-445.

[14] Evans, C. L.; Xie, X. S., Coherent anti-Stokes Raman scattering microscopy: chemical imaging for biology and medicine. [J] *Annu. Rev. Anal. Chem.* **2008,** *1*, 883-909.

[15] Camp Jr, C. H.; Cicerone, M. T., Chemically sensitive bioimaging with coherent Raman scattering. [J] *Nature photonics* **2015,** *9*, 295-305.

[16] Evans, C. L.; Potma, E. O.; Puoris' haag, M.; Côté, D.; Lin, C. P.; Xie, X. S., Chemical imaging of tissue in vivo with video-rate coherent anti-Stokes Raman scattering microscopy. [J] *Proceedings of the National Academy of Sciences* **2005,** *102*, 16807-16812.

[17] Liang, E. J.; Weippert, A.; Funk, J. M.; Materny, A.; Kiefer, W., Experimental observation of surface-enhanced coherent anti-Stokes Raman scattering. [J] *Chemical physics letters* **1994,** *227*, 115-120.

[18] Steuwe, C.; Kaminski, C. F.; Baumberg, J. J.; Mahajan, S., Surface enhanced coherent anti-Stokes Raman scattering on nanostructured gold surfaces. [J] *Nano letters* **2011,** *11*, 5339-5343.

[19] Voronine, D. V.; Sinyukov, A. M.; Hua, X.; Wang, K.; Jha, P. K.; Munusamy, E.; Wheeler, S. E.; Welch, G.; Sokolov, A. V.; Scully, M. O., Time-resolved surface-enhanced coherent sensing of nanoscale molecular complexes. [J] *Scientific reports* **2012,** *2*, 1-5.

[20] Schlücker, S.; Salehi, M.; Bergner, G.; Schütz, M.; Ströbel, P.; Marx, A.; Petersen, I.; Dietzek, B.; Popp, J. r., Immuno-surface-enhanced coherent anti-Stokes Raman scattering microscopy: immunohistochemistry with target-specific metallic nanoprobes and nonlinear Raman microscopy. [J] *Analytical chemistry* **2011,** *83*, 7081-7085.

[21] Yampolsky, S.; Fishman, D. A.; Dey, S.; Hulkko, E.; Banik, M.; Potma, E. O.; Apkarian, V. A., Seeing a single molecule vibrate through time-resolved coherent anti-Stokes Raman scattering. [J] *Nature Photonics* **2014,** *8*, 650-656.

[22] Zhang, Y.; Zhen, Y.-R.; Neumann, O.; Day, J. K.; Nordlander, P.; Halas, N. J., Coherent anti-Stokes Raman scattering with single-molecule sensitivity using a plasmonic Fano resonance. [J] *Nature communications* **2014,** *5*, 4424.

[23] Koo, T.-W.; Chan, S.; Berlin, A. A., Single-molecule detection of biomolecules by surface-enhanced coherent anti-Stokes Raman scattering. [J] *Optics letters* **2005,** *30*, 1024-1026.

[24] Heinrich, C.; Bernet, S.; Ritsch-Marte, M., Wide-field coherent anti-Stokes Raman scattering microscopy. [J] *Applied physics letters* **2004,** *84*, 816-818.

[25] Lei, M.; Winterhalder, M.; Selm, R.; Zumbusch, A., Video-rate wide-field coherent anti-Stokes Raman scattering microscopy with collinear nonphase-matching illumination. [J] *Journal of biomedical optics* **2011,** *16*, 021102.

[26] Toytman, I.; Cohn, K.; Smith, T.; Simanovskii, D.; Palanker, D., Wide-field coherent anti-Stokes Raman scattering microscopy with non-phase-matching illumination. [J] *Optics letters* **2007,** *32*, 1941-1943.

[27] Toytman, I.; Simanovskii, D.; Palanker, D., On illumination schemes for wide-field CARS microscopy. [J] *Optics express* **2009,** *17*, 7339-7347.

[28] Silve, A.; Dorval, N.; Schmid, T.; Mir, L. M.; Attal‐Tretout, B., A wide‐field arrangement for single‐shot CARS imaging of living cells. [J] *Journal of Raman Spectroscopy* **2012,** *43*, 644-650.

[29] Shen, Y.; Wang, J.; Wang, K.; Sokolov, A. V.; Scully, M. O., Wide-field coherent anti-stokes raman scattering

microscopy based on picosecond supercontinuum source. [J] *APL Photonics* **2018,** *3*, 116104.
[30] Fast, A.; Kenison, J. P.; Syme, C. D.; Potma, E. O., Surface-enhanced coherent anti-Stokes Raman imaging of lipids. [J] *Applied optics* **2016,** *55*, 5994-6000.
[31] Kenison, J. P.; Fast, A.; Guo, F.; LeBon, A.; Jiang, W.; Potma, E. O., Imaging properties of surface-enhanced coherent anti-Stokes Raman scattering microscopy on thin gold films. [J] *JOSA B* **2017,** *34*, 2104-2114.
[32] Zong, C.; Xie, Y.; Zhang, M.; Huang, Y.; Yang, C.; Cheng, J.-X., Plasmon-enhanced coherent anti-stokes Raman scattering vs plasmon-enhanced stimulated Raman scattering: Comparison of line shape and enhancement factor. [J] *The Journal of Chemical Physics* **2021,** *154*, 034201.
[33] Lin, H.; Lee, H. J.; Tague, N.; Lugagne, J.-B.; Zong, C.; Deng, F.; Shin, J.; Tian, L.; Wong, W.; Dunlop, M. J., Microsecond fingerprint stimulated Raman spectroscopic imaging by ultrafast tuning and spatial-spectral learning. [J] *Nature communications* **2021,** *12*, 1-12.
[34] Zheng, X.-S.; Hu, P.; Cui, Y.; Zong, C.; Feng, J.-M.; Wang, X.; Ren, B., BSA-coated nanoparticles for improved SERS-based intracellular pH sensing. [J] *Analytical chemistry* **2014,** *86*, 12250-12257.
[35] Zheng, X.-S.; Hu, P.; Zhong, J.-H.; Zong, C.; Wang, X.; Liu, B.-J.; Ren, B., Laser power dependent surface-enhanced Raman spectroscopic study of 4-mercaptopyridine on uniform gold nanoparticle-assembled substrates. [J] *The Journal of Physical Chemistry C* **2014,** *118*, 3750-3757.
[36] Maggioni, M.; Boracchi, G.; Foi, A.; Egiazarian, K., Video denoising, deblocking, and enhancement through separable 4-D nonlocal spatiotemporal transforms. [J] *IEEE Transactions on image processing* **2012,** *21*, 3952-3966.
[37] Behzadi, S.; Serpooshan, V.; Tao, W.; Hamaly, M. A.; Alkawareek, M. Y.; Dreaden, E. C.; Brown, D.; Alkilany, A. M.; Farokhzad, O. C.; Mahmoudi, M., Cellular uptake of nanoparticles: journey inside the cell. [J] *Chemical Society Reviews* **2017,** *46*, 4218-4244.
[38] Zhang, Z.-M.; Chen, S.; Liang, Y.-Z., Baseline correction using adaptive iteratively reweighted penalized least squares. [J] *Analyst* **2010,** *135*, 1138-1146.
[39] Zong, C.; Premasiri, R.; Lin, H.; Huang, Y.; Zhang, C.; Yang, C.; Ren, B.; Ziegler, L. D.; Cheng, J.-X., Plasmon-enhanced stimulated Raman scattering microscopy with single-molecule detection sensitivity. [J] *Nature communications* **2019,** *10*, 1-11.
[40] Premasiri, W. R.; Lee, J. C.; Sauer-Budge, A.; Theberge, R.; Costello, C. E.; Ziegler, L. D., The biochemical origins of the surface-enhanced Raman spectra of bacteria: a metabolomics profiling by SERS. [J] *Analytical and bioanalytical chemistry* **2016,** *408*, 4631-4647.
[41] Frontiera, R. R.; Henry, A.-I.; Gruenke, N. L.; Van Duyne, R. P., Surface-enhanced femtosecond stimulated Raman spectroscopy. [J] *The journal of physical chemistry letters* **2011,** *2*, 1199-1203.

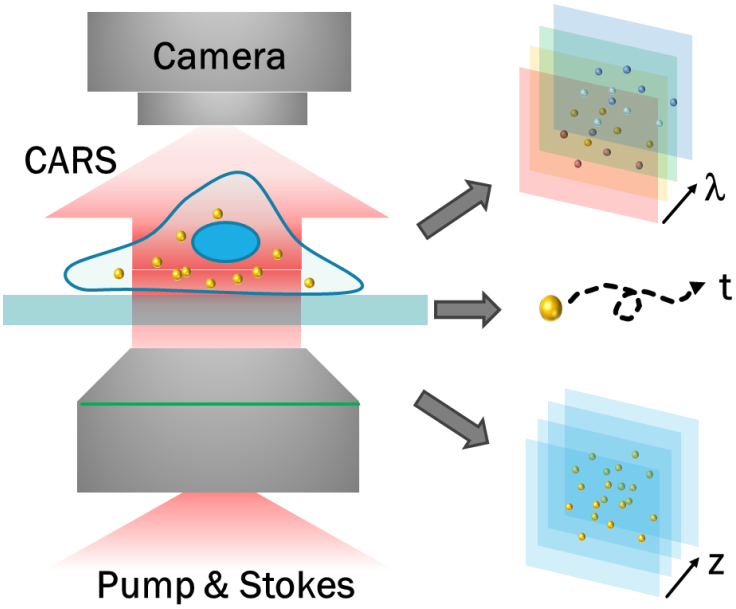

Table of Content Figure